Oxidation product characterization from ozonolysis of the diterpene ent-kaurene

Yuanyuan Luo[1], Olga Garmash[1,2], Haiyan Li[1,3], Frans Graeffe[1], Arnaud P. Praplan[4], Anssi Liikanen[4], Yanjun Zhang[1,5], Melissa Meder[1], Otso Peräkylä[1], Josep Peñuelas[6,7], Ana María Yáñez-Serrano[6,7,8], Mikael Ehn[1]

[1]Institute for Atmospheric and Earth System Research/Physics, Faculty of Science, University of Helsinki, Helsinki, 00014, Finland
[2]Aerosol Physics Laboratory, Physics Unit, Tampere University, Tampere, 33014, Finland
[3]School of Civil and Environmental Engineering, Harbin Institute of Technology, Shenzhen, 518055, China
[4]Atmospheric Composition Research, Finnish Meteorological Institute, Helsinki, 00101, Finland
[5]Univ Lyon, Université Claude Bernard Lyon 1, CNRS, IRCELYON, Villeurbanne, 69626, France
[6]CREAF, Bellaterra (Cerdanyola del Vallès), Catalonia, E08193, Spain
[7]CSIC, Global Ecology Unit, CREAF-CSIC-UAB, Bellaterra (Cerdanyola del Vallès), Catalonia, E08193, Spain
[8]IDAEA-CSIC, Barcelona, 08034, Spain

Correspondence to: Yuanyuan Luo (yuanyuan.luo@helsinki.fi) and Mikael Ehn (mikael.ehn@helsinki.fi)

Table S1. Sampling details and kaurene quantification for Tenax tubes.

No.	Sampling start time	Sampling end time	Volume (L)	Kaurene mass (ng)	Kaurene concentration (ppb)
1	01-15 10:08:49	01-15 10:36:12	5.29	1.51	0.03
2	01-15 14:52:50	01-15 15:16:53	4.95	62.10	1.13
3	01-28 11:30:28	01-28 12:00:53	5.64	0.89	0.01
4	01-28 13:36:54	01-28 13:56:51	3.74	299.59	7.20

Text S1. Determination of reaction rate coefficient of kaurene with ozone.

There are only a few studies concerning the reaction rate coefficient of diterpenes with O_3. Moreover, reported reaction rate coefficients span two orders of magnitude between the values given by Helin et al. (2020) and EPI Suite (Environmental Protection Agency, United States). In order to estimate the reaction rate coefficient of kaurene with O_3 from our own experiments, we constructed a simple kinetic model. The model predicted kaurene and O_3 concentrations using several different kaurene-O_3 reaction rate coefficients. By comparing the trends in simulated and measured kaurene and O_3, we could estimate the reaction rate coefficient of kaurene ozonolysis, as described below.

To estimate the reaction rate coefficient, we chose the experiment conducted on January 15th (from 12:00 to 3:00 the next day). During that experiment, both O_3 and kaurene were introduced to the chamber at high concentrations, the Vocus had a constant FIMR pressure, and no seed particles were injected. In the model, the injection was set as the only source for both

kaurene and O_3. The loss term of kaurene and O_3 included the flush-out and chemical reactions. Hydroxyl radical (OH) can be formed from ozonolysis of alkenes; thus, we also considered OH reactions with kaurene in the model.

In our model, the concentration of species X (i.e., kaurene, O_3, and OH) at time j equals the concentration at the previous time point (j-1), plus relevant injection/formation rates, minus losses from chemical reactions and flush-out. Therefore, the concentration of kaurene (kau), O_3, and OH with 0.01 s time resolution can be modeled as follows:

$$O_3(j) = O_3(j\text{-}1) + 0.01*(k_{in}*O_{3,in} - k_1*kau(j\text{-}1)*O_3(j\text{-}1) - k_2*OH(j\text{-}1)*O_3(j\text{-}1) - k_{flush\text{-}out}*O_3(j\text{-}1)) \quad (S1)$$

$$kau(j) = kau(j\text{-}1) + 0.01*(k_{in}*kau_{in} - k_1*kau(j\text{-}1)*O_3(j\text{-}1) - k_3*OH(j\text{-}1)*kau(j\text{-}1) - k_{flush\text{-}out}*kau(j\text{-}1)) \quad (S2)$$

$$OH(j) = OH(j\text{-}1) + 0.01*(y*k_1*kau(j\text{-}1)*O_3(j\text{-}1) - k_2*OH(j\text{-}1)*O_3(j\text{-}1) - k_3*OH(j\text{-}1)*kau(j\text{-}1) - k_{flush\text{-}out}*OH(j\text{-}1)) \quad (S3)$$

The average residence time in the COALA chamber was 56 min, and the injection rate k_{in} equals the flush-out rate, i.e. $k_{in} = k_{flush\text{-}out} = 1/(56\ min) = 3\times10^{-4}\ s^{-1}$. $O_{3,in}$, and kau_{in} represent the injected amount of O_3 and kaurene, respectively. k_1, k_2, and k_3 are the reaction rate coefficients of kaurene-O_3, OH-O_3, and kaurene-OH, respectively. Out of these, only $k_2 = 7.3\times10^{-14} cm^3 molec^{-1} s^{-1}$ is well known (Atkinson et al., 2004). y is the OH yield from the reaction of kaurene and O_3. In summary, the unknown parameters in the model are kau_{in}, kau, k_1, k_3, and y. However, we can utilize the knowledge of the relative changes of the kaurene and O_3 concentrations upon changes in input parameters to constrain the ranges of the different parameters.

The modeled experiment consisted of three stages, as shown by the solid lines in Fig. S1. First, kaurene was added without any O_3 into the chamber around 12:00. Second, after ~3 h, O_3 addition began ($O_{3,in}$ = 72.5 ppb). kaurene reacted with O_3 and kaurene concentration in the chamber reduced. Third, kaurene injection was stopped 5 h later, and kaurene concentration decayed, while ozone concentration slightly increased. We modeled the concentration of kaurene and O_3 in the chamber with different values for the unknown parameters (non-solid traces in Fig. S1). It should be noted that the modeled injection of kaurene at the first stage started around 30 min later than the real injection. The reason for this was that the kaurene response in the chamber was always slower than in the model, presumably due to interactions with the walls of the chamber and tubing. Matching the relative changes of O_3 and kaurene between simulation and measurement during the second and third stages was the main criteria for determining the reaction rate coefficient.

We tested three kaurene-O_3 reaction rate coefficients (k_1), with varying rate coefficients of kaurene-OH reaction (k_3), OH yield (y), and input amount of kaurene (kau_{in}). The input parameters of different tests are listed in Table S2, and the results are shown in Fig. S1. As can be seen from the figures, out of all the tested values, y=0.5 and $k_1=5\times10^{-16} cm^3 molec^{-1} s^{-1}$ gave the best simulation of the relative kaurene decay upon O_3 addition in all cases. With these premises, we can then try to estimate k_3 and kau_{in}. The kaurene decay was not very sensitive to k_3, with a reasonable agreement for all the modeled values, despite ranging over two orders of magnitude. This partly suggests that the formed OH mainly reacts with other compounds (e.g., contaminants) than kaurene in our chamber. However, the relative increase in O_3 when kaurene was removed around midnight

shows a larger difference with different combinations of k_3 and kau_{in}. It is not possible for us to determine these values exactly, partly because the kaurene concentration had not fully stabilized before the O_3 injection, thus bringing uncertainty to the final kaurene concentration that would have been achieved without O_3. However, as a general conclusion, the best agreement between the kaurene and O_3 changes comes with a kau_{in} close to the modeled 5.3 ppb, being slightly lower if k_3 was 10^{-12} $cm^3molec^{-1}s^{-1}$ and slightly higher if k_3 was closer to 10^{-11} $cm^3molec^{-1}s^{-1}$. We therefore chose $k_3=1\times10^{-11}cm^3molec^{-1}s^{-1}$ as a reasonable value based on our data, but again conclude that this value is less important for our study. The main result was that we were able to estimate a good value for the kaurene- O_3 reaction rate coefficient of $k_1=5\times10^{-16}cm^3molec^{-1}s^{-1}$. This value was then used to derive the correction factors for the kaurene concentrations measured by the Vocus (Sect. 2.3 in the main text).

Table S2. Input parameters. k_1 refers to the reaction rate coefficient of kaurene-O_3, and k_3 to reaction rate coefficient of kaurene-OH.

Parameter	Modeled values
Kaurene injection in ppb (kau_{in})	1.6, 5.3, 10.6
k_1 ($cm^3molec^{-1}s^{-1}$)	1×10^{-15}, 5×10^{-16}, 1×10^{-16}
k_3 ($cm^3molec^{-1}s^{-1}$)	1×10^{-10}, 1×10^{-11}, 1×10^{-12}
OH yield (y)	1, 0.5

[1]Kaurene injection, kau_{in}: the injected concentration of kaurene was unknown due to the lack of any authentic diterpene standards. Thus, we used different kaurene concentrations to do the tests. The three values of kaurene injection shown here were determined so that the peak concentrations of kaurene could be close to 1.5 ppb, 5 ppb and 10 ppb in the end of the first stage.

[2]k_1 was reported to be $2.4\times10^{-15}cm^3molec^{-1}s^{-1}$ by Helin et al. (2020) and $1.2\times10^{-17}cm^3molec^{-1}s^{-1}$ by EPI Suite. Thus, we test three k_1 values within the range of 1×10^{-15} – $1\times10^{-16}cm^3molec^{-1}s^{-1}$.

[3]The range of reaction rate coefficient of kaurene-OH, k_3 for testing was determined based on the reported results of monoterpenes and sesquiterpenes.

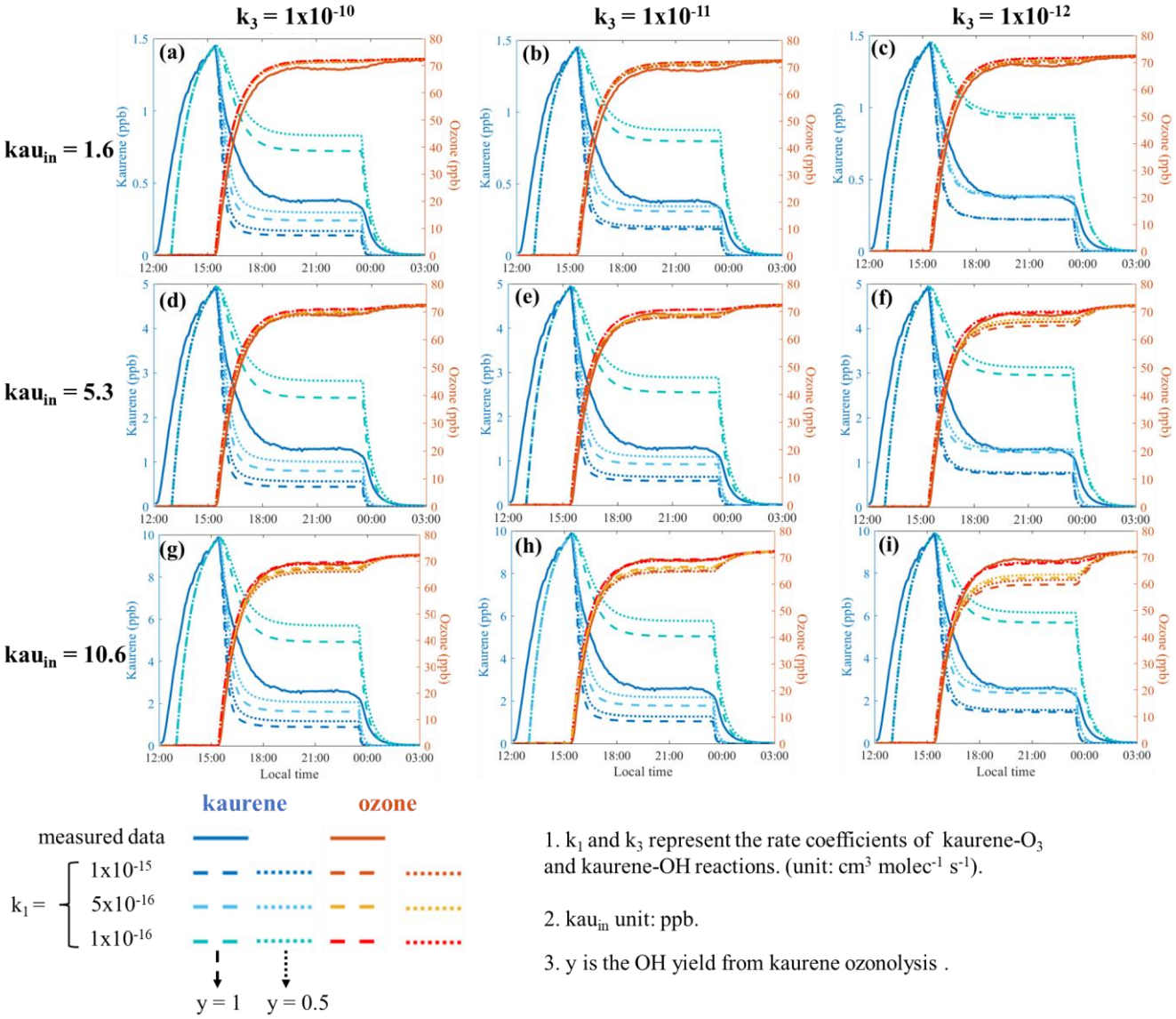

Figure S1. Model results. Panels (a), (b), and (c) show the results when injected kaurene was set as 1.6 ppb; panels (d), (e), and (f) are the results when we set the injected kaurene to 5.3 ppb; panels (g), (h), and (i) show the model results when 10.6 ppb kaurene was injected. Note that the raw data of the Vocus was scaled roughly to match the modeled concentration and referred to as measured kaurene (blue solid lines) in these plots. We use different kinds of blue to show the trends of kaurene and orange for O_3. The same color represents the same value of k_1 in the tests. The dashed lines in all panels show the results at y=1, while the dotted lines are at y=0.5.

Table S3. Products of kaurene oxidation as identified in the Vocus. Data correspond to Fig. 4b in the main text. All ions are positively charged and shown including the reagent ion (H^+). f is the fraction of the total signal.

C	H	O	N	m/z, Th	f×10^8	C	H	O	N	m/z, Th	f×10^8
10	15	0	0	135.1170	30.3	18	29	2	0	277.2152	1.3
11	17	0	0	149.1326	70.6	19	33	1	0	277.2519	0.1
12	19	0	0	163.1482	88.6	20	31	1	0	287.2363	1.1
13	21	0	0	177.1638	113.8	19	29	2	0	289.2152	0.9
14	23	0	0	191.1794	34.3	20	33	1	0	289.2519	2.4
15	23	0	0	203.1794	16.6	20	36	0	1	290.2839	44.1
16	25	0	0	217.1950	35.7	19	31	2	0	291.2308	17.7
18	25	0	0	241.1950	0.3	19	34	1	1	292.2628	20.1
19	29	0	0	257.2262	16.4	19	33	2	0	293.2464	18.1
19	31	0	0	259.2418	1.2	20	31	2	0	303.2308	0.9
19	33	0	0	261.2574	0.8	19	29	3	0	305.2097	0.3
19	27	1	0	271.2051	0.6	20	33	2	0	305.2464	0.6
20	31	0	0	271.2418	19.1	19	31	3	0	307.2253	0.2
20	32	0	0	272.2496	25.1	20	35	2	0	307.2620	0.4
19	29	1	0	273.2207	3.4	19	34	2	1	308.2573	5.4
20	33	0	0	273.2574	867.7	19	33	3	0	309.2409	1.4
19	30	1	0	274.2285	24.5	20	31	3	0	319.2253	0.3
19	31	1	0	275.2363	31.9	20	33	3	0	321.2409	36.0

Table S4. Products of kaurene oxidation as identified in nitrate CI-APi-TOF spectra. Data correspond to Fig. 4 c and d in the main text. All ions are negatively charged and shown including the reagent ion (NO_3^-). f is the fraction of the total signal.

C	H	O	N	m/z, Th	f×10^7	C	H	O	N	m/z, Th	f×10^7
19	28	7	1	382.1858	47.0	24	37	10	1	499.2407	3.3
18	28	8	1	386.1807	45.0	24	38	10	1	500.2485	1093.4
19	32	7	1	386.2170	68.5	25	42	9	1	500.2848	14.4
20	30	7	1	396.2014	96.5	19	26	15	1	508.1294	3.1
19	28	8	1	398.1807	39.6	20	30	14	1	508.1657	31.3
18	26	9	1	400.1600	19.0	21	34	13	1	508.2020	8.6
19	30	8	1	400.1963	98.7	23	27	12	1	509.1525	56.2
19	31	8	1	401.2041	3.5	20	31	14	1	509.1735	44.6
18	28	9	1	402.1756	44.9	19	28	15	1	510.1450	10.4
19	32	8	1	402.2119	422.4	20	32	14	1	510.1813	11.0
19	33	8	1	403.2197	2.3	19	30	15	1	512.1606	6.1
20	30	8	1	412.1963	1086.4	20	34	14	1	512.1969	4.4
19	28	9	1	414.1756	694.5	25	38	10	1	512.2485	79.0
20	32	8	1	414.2119	40.1	26	42	9	1	512.2848	16.5
19	29	9	1	415.1834	6.9	24	36	11	1	514.2278	618.5
20	33	8	1	415.2197	11.9	25	40	10	1	514.2641	25.9
18	26	10	1	416.1549	25.3	23	34	12	1	516.2071	3.4
19	30	9	1	416.1912	171.9	21	32	14	1	522.1813	3.9
20	34	8	1	416.2275	50.9	23	40	12	1	522.2539	8.2
19	31	9	1	417.1990	67.5	20	30	15	1	524.1606	18.8
18	28	10	1	418.1705	61.4	26	38	10	1	524.2485	31.6
19	32	9	1	418.2068	115.4	27	42	9	1	524.2848	277.7
18	30	10	1	420.1861	58.3	20	32	15	1	526.1762	10.5
19	26	10	1	428.1549	10.8	26	40	10	1	526.2641	526.7
20	30	9	1	428.1912	312.9	27	44	9	1	526.3004	2.1
21	34	8	1	428.2275	2.2	19	30	16	1	528.1555	3.1
19	27	10	1	429.1627	6.8	25	38	11	1	528.2434	98.2
20	31	9	1	429.1990	15.6	26	42	10	1	528.2797	54.5
19	28	10	1	430.1705	122.5	25	40	11	1	530.2590	26.7
20	32	9	1	430.2068	77.2	24	38	12	1	532.2383	7.0
19	29	10	1	431.1783	90.5	25	42	11	1	532.2746	3.5
20	33	9	1	431.2146	9.6	27	40	10	1	538.2641	122.6
18	26	11	1	432.1498	21.4	28	44	9	1	538.3004	282.6
19	30	10	1	432.1861	554.0	26	38	11	1	540.2434	8.7

20	34	9	1	432.2224	13.8	27	42	10	1	540.2797	248.6
18	27	11	1	433.1576	52.1	28	46	9	1	540.3160	1.9
19	31	10	1	433.1939	40.3	26	40	11	1	542.2590	69.4
18	28	11	1	434.1654	62.0	27	44	10	1	542.2953	14.8
19	32	10	1	434.2017	96.7	24	33	13	1	543.1942	5.6
18	29	11	1	435.1732	37.5	27	45	10	1	543.3031	1.4
19	33	10	1	435.2095	4.3	22	26	15	1	544.1294	1.5
20	28	10	1	442.1705	7.6	25	38	12	1	544.2383	15.9
21	32	9	1	442.2068	76.8	26	42	11	1	544.2746	4.2
22	36	8	1	442.2431	6.3	23	38	14	1	552.2281	2.0
20	30	10	1	444.1861	882.8	24	42	13	1	552.2644	6.1
21	34	9	1	444.2224	15.5	28	42	10	1	552.2797	20.5
20	31	10	1	445.1939	43.7	29	46	9	1	552.3160	13.7
21	35	9	1	445.2302	9.1	27	40	11	1	554.2590	141.8
19	28	11	1	446.1654	1904.3	28	44	10	1	554.2953	88.7
20	32	10	1	446.2017	132.9	26	38	12	1	556.2383	5.7
18	25	12	1	447.1369	20.9	27	42	11	1	556.2746	107.7
19	29	11	1	447.1732	31.1	28	46	10	1	556.3109	3.7
20	33	10	1	447.2095	8.8	24	40	14	1	566.2437	3.2
18	26	12	1	448.1447	18.9	29	44	10	1	566.2953	28.2
19	30	11	1	448.1810	173.6	28	42	11	1	568.2746	66.3
20	34	10	1	448.2173	19.1	29	46	10	1	568.3109	88.4
18	27	12	1	449.1525	33.1	27	40	12	1	570.2539	11.1
19	31	11	1	449.1888	66.0	28	44	11	1	570.2902	136.4
18	28	12	1	450.1603	102.7	29	48	10	1	570.3265	20.0
19	32	11	1	450.1966	31.1	27	42	12	1	572.2695	23.6
18	29	12	1	451.1681	21.8	28	46	11	1	572.3058	3.7
22	34	9	1	456.2224	550.4	29	44	11	1	582.2902	53.5
23	38	8	1	456.2587	6.3	28	42	12	1	584.2695	15.8
20	28	11	1	458.1654	9.1	29	46	11	1	584.3058	78.9
21	32	10	1	458.2017	5.4	26	36	14	1	586.2125	3.0
22	36	9	1	458.2380	7.2	28	44	12	1	586.2851	25.7
19	26	12	1	460.1447	20.1	27	42	13	1	588.2644	16.9
20	30	11	1	460.1810	227.9	29	50	11	1	588.3370	5.6
21	34	10	1	460.2173	6.1	26	40	14	1	590.2437	2.6
19	27	12	1	461.1525	18.1	27	44	13	1	590.2800	3.3
20	31	11	1	461.1888	64.8	28	48	12	1	590.3163	0.8

18	24	13	1	462.1240	9.1	29	42	12	1	596.2695	2.6
19	28	12	1	462.1603	97.1	28	40	13	1	598.2488	1.0
20	32	11	1	462.1966	87.3	29	44	12	1	598.2851	30.2
18	25	13	1	463.1318	11.1	27	38	14	1	600.2281	0.7
19	29	12	1	463.1681	73.5	28	42	13	1	600.2644	8.7
20	33	11	1	463.2044	23.3	29	46	12	1	600.3007	12.2
18	26	13	1	464.1396	11.9	27	40	14	1	602.2437	2.7
19	30	12	1	464.1759	172.4	28	44	13	1	602.2800	6.3
20	34	11	1	464.2122	15.8	29	48	12	1	602.3163	4.1
19	31	12	1	465.1837	17.2	27	42	14	1	604.2593	6.3
18	28	13	1	466.1552	26.7	29	50	12	1	604.3319	2.7
19	32	12	1	466.1915	18.1	29	46	14	1	632.2905	6.5
19	26	13	1	476.1396	3.8	29	44	15	1	646.2698	3.8
20	30	12	1	476.1759	127.5	37	58	9	1	660.4096	10.8
21	34	11	1	476.2122	9.1	38	60	9	1	674.4252	83.6
19	27	13	1	477.1474	20.3	38	58	10	1	688.4045	3.3
20	31	12	1	477.1837	55.4	39	62	9	1	688.4408	15.8
21	35	11	1	477.2200	1.1	40	66	8	1	688.4771	0.2
19	28	13	1	478.1552	479.6	38	60	10	1	690.4201	8.9
20	32	12	1	478.1915	75.8	39	64	9	1	690.4564	5.4
19	29	13	1	479.1630	44.4	40	68	8	1	690.4927	0.6
20	33	12	1	479.1993	7.7	37	58	11	1	692.3994	9.4
18	26	14	1	480.1345	14.7	38	62	10	1	692.4357	0.5
19	30	13	1	480.1708	42.3	39	66	9	1	692.4720	1.1
20	34	12	1	480.2071	9.7	38	58	11	1	704.3994	7.2
18	27	14	1	481.1423	3.4	39	62	10	1	704.4357	4.7
19	31	13	1	481.1786	6.3	40	66	9	1	704.4720	1.3
19	32	13	1	482.1864	11.4	38	60	11	1	706.4150	18.9
22	32	11	1	486.1966	1.2	39	64	10	1	706.4513	10.0
23	36	10	1	486.2329	100.2	37	58	12	1	708.3943	4.4
24	40	9	1	486.2692	1.4	38	62	11	1	708.4306	7.1
19	26	14	1	492.1345	8.0	38	58	12	1	720.3943	2.9
20	30	13	1	492.1708	55.7	39	62	11	1	720.4306	9.7
21	34	12	1	492.2071	5.2	38	60	12	1	722.4099	7.5
19	27	14	1	493.1423	4.7	39	64	11	1	722.4462	11.6
20	31	13	1	493.1786	37.7	37	58	13	1	724.3892	4.3
21	35	12	1	493.2149	4.1	38	62	12	1	724.4255	3.8

19	28	14	1	494.1501	24.7	38	58	13	1	736.3892	5.5
20	32	13	1	494.1864	27.6	39	62	12	1	736.4255	8.1
21	36	12	1	494.2227	0.6	38	60	13	1	738.4048	6.5
20	33	13	1	495.1942	16.2	39	64	12	1	738.4411	5.2
19	30	14	1	496.1657	16.5	38	58	15	1	768.3790	2.6
20	34	13	1	496.2020	10.8	39	62	14	1	768.4153	6.0
19	32	14	1	498.1813	5.7	40	66	13	1	768.4516	0.8
24	36	10	1	498.2329	200.0	40	66	14	1	784.4465	2.3
25	40	9	1	498.2692	10.2	40	64	15	1	798.4258	2.2

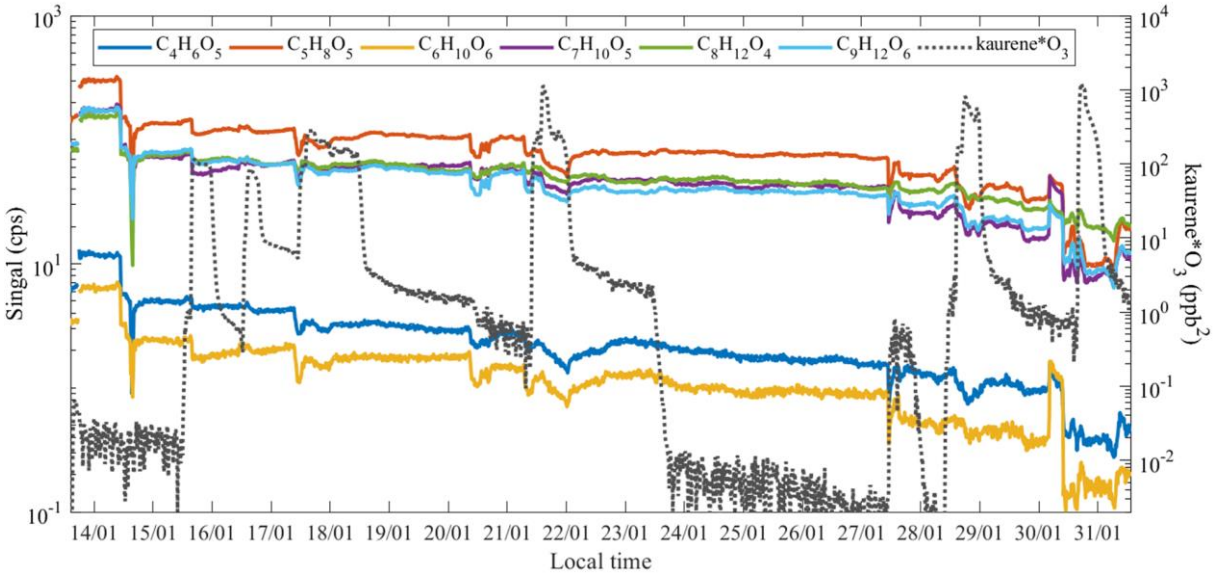

Figure S2. Temporal behaviors of the main contaminants. The most abundant contaminant in each group with different carbon numbers is shown here. $C_8H_{12}O_4$ was detected by Vocus, while the other five contaminants shown here were detected by nitrate CI-APi-TOF. The dark gray dashed line depicts the kaurene ozonolysis rate (kaurene*O_3 in the right y-axis).

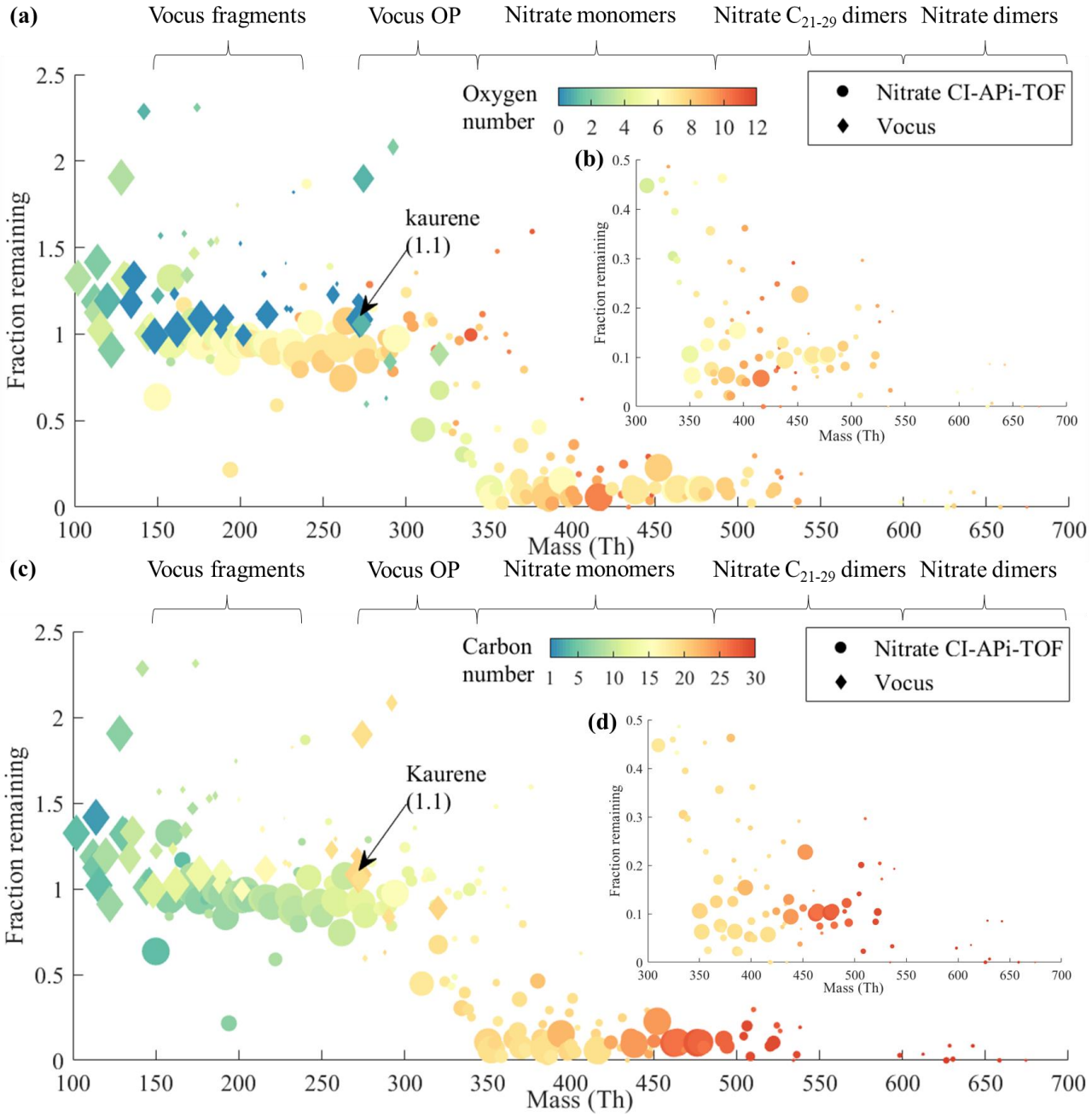

Figure S3. Seed injection behaviour. The fraction remaining factor corresponds to the ratio of the signal after seed particles injection to seed removal. The molar mass indicated on the x-axis is without the reagent ions. The color indicates the carbon numbers in the composition. The area of circles and diamonds is scaled linearly to the magnitude of each compound's signal when there were no seed particles in the chamber. Compounds with average signal intensities (during the steady state before seed injection) below three times the standard deviation are excluded from the plots. The text at the top shows roughly which compound groups are found in

which parts of the mass range. The 'Vocus fragments' refers to the kaurene fragments, and 'Vocus OP' refers to C_{18-20} oxidation products. 'Nitrate monomers', 'Nitrate C_{21-29} dimers', and 'Nitrate dimers' represent the C_{18-20} HOM monomers, C_{21-29} HOM dimers, and C_{37-40} HOM dimers measured with nitrate CI-APi-TOF, respectively. The zoomed-in views of the mass range above 300 Th are shown in panels (b) and (d).

References

Atkinson, R., Baulch, D. L., Cox, R. A., Crowley, J. N., Hampson, R. F., Hynes, R. G., Jenkin, M. E., Rossi, M. J., and Troe, J.: Evaluated kinetic and photochemical data for atmospheric chemistry: Volume I - gas phase reactions of Ox, HOx, NOx and SOx species, Atmospheric Chemistry and Physics, 4, 1461-1738, 10.5194/acp-4-1461-2004, 2004.

Helin, A., Hakola, H., and Hellén, H.: Optimisation of a thermal desorption–gas chromatography–mass spectrometry method for the analysis of monoterpenes, sesquiterpenes and diterpenes, Atmospheric Measurement Techniques 13, 3543-3560, 10.5194/amt-13-3543-2020, 2020.